Asian Journal of Chemistry; Vol. 33, No. 8 (2021), 1861-1867

ASIAN JOURNAL OF CHEMISTRY

https://doi.org/10.14233/ajchem.2021.23258

Synthesis, Spectroscopic Properties and Hirshfeld Surface Analysis of 3,14-Dimethyl-2,6,13,17-tetraazoniatricyclo(16.4.0.0^{7,12})docosane Tetrachloride Tetrahydrate

SUNGHWAN JEON[1], JÁN MONCOL[2], MILAN MAZÚR[2], MARIÁN VALKO[2], KEON SANG RYOO[1,*] and JONG-HA CHOI[1,*]

[1]Department of Chemistry, Andong National University, Andong 36729, Republic of Korea
[2]Department of Chemistry, Faculty of Chemical and Food Technology, Slovak University of Technology, SK-81237 Bratislava, Slovakia

*Corresponding authors: E-mail: jhchoi@anu.ac.kr; ksr@anu.ac.kr

Received: 22 April 2021; *Accepted*: 5 June 2021; *Published online*: 26 July 2021; AJC-20439

Single crystals of 3,14-dimethyl-2,6,13,17-tetraazoniatricyclo(16.4.0.0^{7,12})docosane tetrachloride tetrahydrate compound, $[C_{20}H_{44}N_4]Cl_4{\cdot}4H_2O$ (**1**), were obtained by a novel synthetic route and characterized by elemental analysis and X-ray diffraction. The synthesized compound crystallized in the monoclinic space group $P2_1/n$ with two molecules of compound **1** in the unit cell [a = 7.5548(3) Å, b = 23.1838(8) Å, c = 8.3101(4) Å; β = 103.390(3)°]. The asymmetric unit contains half a centrosymmetric macrocyclic cation, two chloride anions and two water molecules. The organic $[C_{20}H_{44}N_4]^{4+}$ fragment of **1** adopts an exodentate [3,4,3,4]-*D* conformation. The C–C and N–C bond lengths of the macrocyclic tetracation range 1.525(3)-1.540(3) Å and 1.505(3)-1.519(3) Å, respectively. A three-dimensional hydrogen bonding network provides crystal cohesion through O–H···Cl, N–H···Cl and N–H···O interactions between organic cations, chloride anions and water molecules. The functional groups present in the crystal were studied by Fourier-transform infrared spectroscopy and Raman spectroscopy. The Hirshfeld surface analysis and 2D fingerprint plots revealed that the crystal packing in **1** is dominated by H···H, Cl···H/H···Cl and O···H/H···O contacts.

Keywords: Characterization, Macrocycle, Endodentate, Tetrachloride, Spectral properties, Hirshfeld surface analysis.

INTRODUCTION

In recent years, compounds containing cyclam (1,4,8,11-tetraazacyclotetradecane, $C_{10}H_{24}N_4$) and cyclam derivatives have shown a potential inhibitory effect on human immunodeficiency virus (HIV) replication and the ability to mobilize hematopoietic progenitor stem cells from the bone marrow into the blood [1-3]. To develop new cyclam containing transition metal based anti-HIV drugs, more information about their configuration and crystal packing forces is essential [4], especially to develop drugs which target different events in the HIV replicative cycle. The macrocycle 3,14-dimethyl-2,6,13,17-tetraazatricyclo(16.4.0.0^{7,12})docosane ($C_{20}H_{40}N_4$, L) contains a cyclam backbone with two cyclohexane subunits and two methyl groups located at the alpha positions on the propyl chain. Macrocycle L is a basic amine capable of forming the dication $[C_{20}H_{42}N_4]^{2+}$ (H_2L^{2+}) or tetracation $[C_{20}H_{44}N_4]^{4+}$ (H_4L^{4+}), in which all the N–H bonds are generally available for hydrogen bonding. It is known that L and H_2L^{2+} dication adopt endodentate conformations along the center of the macrocyclic cavity [5-9]. The stabilization of the endodentate conformation can be attributed to strong intramolecular N–H···N hydrogen bonds. Unlike L and H_2L^{2+} dication, H_4L^{4+} tetracation adopts an exodentate conformation. Furthermore, 14-membered cyclam moiety of the tetracation can adopt four exodentate [3,4,3,4]-[*A*~*D*] conformations depending on the counter anion (Fig. 1). The numbers in Fig. 1 represent the number of bonds on each side of the rectangle.

The solid-state structures of naphthalenemethanol ($C_{10}H_7CH_3OH$) [5] and nitric acid (NO_2OH) [6] adducts of L and several salts of its dication (H_2L^{2+}), including sulfate [7], tricyanoferrous [8] and bromide [9] have been reported. In a recent communication, we reported the solid-state structure of $[C_{20}H_{44}N_4]Cl_4{\cdot}4H_2O$ (**1**) determined by single-crystal synchrotron radiation X-ray diffraction data [10]. However, its detailed physical properties have not yet been reported.

In this article, we describe a new preparation and physicochemical characterization of compound **1**, $[C_{20}H_{44}N_4]Cl_4{\cdot}4H_2O$. To evaluate the nature and proximity of the interactions present in the solid-state packing, detailed analyses of the Hirshfeld surface and fingerprint plots were also performed.

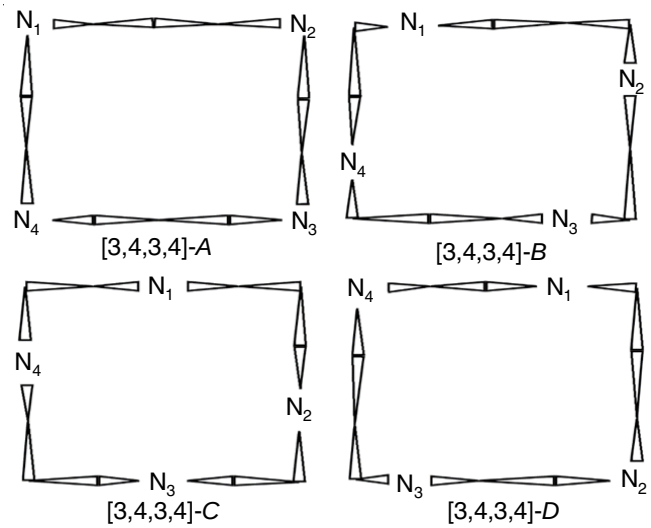

Fig. 1. Four possible exodentate conformations of the cyclam moiety

EXPERIMENTAL

Synthesis and crystallization: Commercially available *trans*-1,2-cyclohexanediamine and methyl vinyl ketone (Sigma-Aldrich) were used as obtained. All reagents were of analytical grade and used as received without further purification. The starting material, 3,14-dimethyl-2,6,13,17-tetraazatricyclo-(16.4.0.0^{7,12})docosane (L), was synthesized according to a reported method [11]. A 50 mL solution of 0.5 mmol $CuBr_2$ was prepared, from which a 20 mL aliquot was replaced by the macrocycle L (0.091 g, 0.25 mmol). The resulting solution was refluxed for 1 h at 373 K and then cooled to 298 K. Subsequently, the pH was adjusted to 3.0 by the addition of 1.0 M HCl and the solution was left at room temperature. Colourless and violet crystals were formed within the solution over the next few days. The product mixture was added to 30 mL of MeOH-acetone (1:2) solution under stirring and stirring was continued for 30 min at room temperature. The obtained mixture was filtered to remove the violet component $[Cu(L)(H_2O)_2]Br_2$ [12] and compound **1** was obtained as large colourless block crystals, which were suitable for single-crystal X-ray diffraction analysis. Anal. calcd. (found) % for $C_{20}H_{44}N_4O_4Cl_4$: C, 43.32 (43.41); H, 9.46 (9.58); N, 10.11 (10.24).

Measurements of physical properties: UV-visible absorption spectrum was recorded using an HP 8453 diode array spectrophotometer. The mid-infrared spectrum (KBr pellet) was recorded using a JASCO 460 plus series Fourier-transform infrared (FT-IR) spectrometer. Raman measurement was performed using Bruker RFS 27 "MultiRam" FT-Raman spectrometer (Bruker, Karlsruhe, FRG) with Nd:YAG laser at the wavelength of 1064 nm. Electron paramagnetic resonance (EPR) spectra of the powdered compounds were recorded on an X-band (~9.4 GHz) EMX series EPR spectrometer. Analyses for C, H and N were performed using a Perkin-Elmer 2400II CHNS/O analyzer.

X-ray structural determination: X-ray diffraction data of the colourless crystals of **1** (0.26 mm × 0.25 mm × 0.242 mm) were collected on a Stoe StadiVari diffractometer at 100(2) K using Cu*K*α radiation (λ = 1.54186 Å) from a microfocused Xenocs Genix3D Cu HF source and a Pilatus3R 300K HPAD detector. The diffraction intensities were corrected using the Lorentz and polarization factors. The crystal structure of **1** was solved using the SHELXT-2018 [13] program and refined by the full-matrix least-squares method in SHELXL-2018 [14]. Multi-scan absorption corrections were applied using the Stoe LANA software [15]. Molecular graphics were produced using DIAMOND-3 software [16]. Non-hydrogen atoms were refined anisotropically; hydrogen atoms were located on a difference map, N–H hydrogen atoms were then refined with distance restraints and C–H hydrogen atoms were constrained to ride on the parent carbon atom, with C–H = 0.98 Å and U_{iso}(H) = 1.5U_{eq}(C) for the methyl groups and C–H = 0.99 Å and U_{iso}(H) = 1.2U_{eq}(C) for the methylene groups. Crystal data, data collection and structure refinement details are summarized in Table-1.

TABLE-1
CRYSTALLOGRAPHIC DATA FOR **1**

Crystal data	
Chemical formula	$[C_{20}H_{44}N_4]Cl_4{\cdot}4H_2O$
M_r	554.45
Crystal system, space group	Monoclinic, $P2_1/n$
Temperature (K)	100(2)
a, b, c (Å)	7.5548(3), 23.1838(8), 8.3101(4)
β (°)	103.390(3)
V (Å^3)	1415.94(10)
Z	2
Radiation type	Cu Kα radiation, λ = 1.54186 Å
μ (mm^{-1})	4.05
Crystal size (mm)	0.26 × 0.25 × 0.24
Data collection	
Diffractometer	Stoe Stadivari with Xenocs Genix3D Cu HF
Absorption correction	Multi-scan [15]
T_{min}, T_{max}	0.157, 0.443
No. of measured, independent and observed [I>2σ(I)] reflections	11956, 2701, 2486
R_{int}	0.032
$(\sin\theta/\lambda)_{max}$ (Å^{-1})	0.616
Refinement	
R[F^2 > 2σ(F^2)], wR(F^2), S	0.044, 0.125, 1.07
No. of reflections	2701
No. of parameters	152
No. of restraints	0
H-atom treatment	H-atoms parameters constrained
$\Delta\rho_{max}$, $\Delta\rho_{min}$ (e Å^{-3})	0.66, -0.36

RESULTS AND DISCUSSION

Spectroscopic studies: FT-IR and Raman spectroscopies were used to identify the functional groups present in the solid-state and to obtain information about the solid-state structure. The IR and Raman spectra of 3,14-dimethyl-2,6,13,17-tetraazoniatricyclo(16.4.0.0^{7,12})docosane tetrachloride tetrahydrate (**1**) are shown in Figs. 2 and 3, respectively.

Detailed assignment of the main bands observed in the IR and Raman spectra of **1** are summarized in Table-2. Tentative assignments were made according to literature data [17-19].

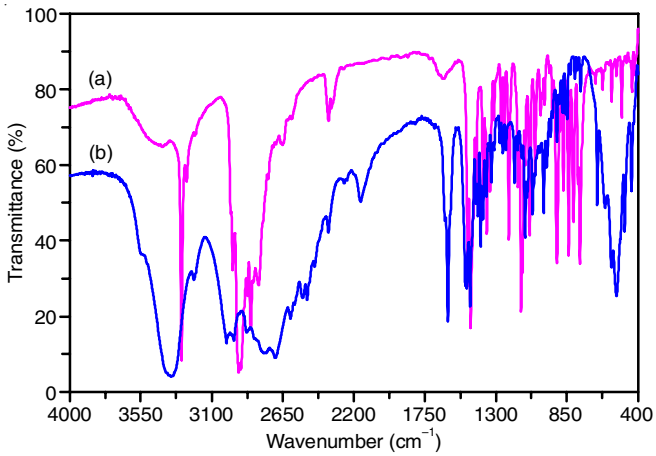

Fig. 2. FT-IR spectra of (a) free L (pink line) and (b) **1** (blue line)

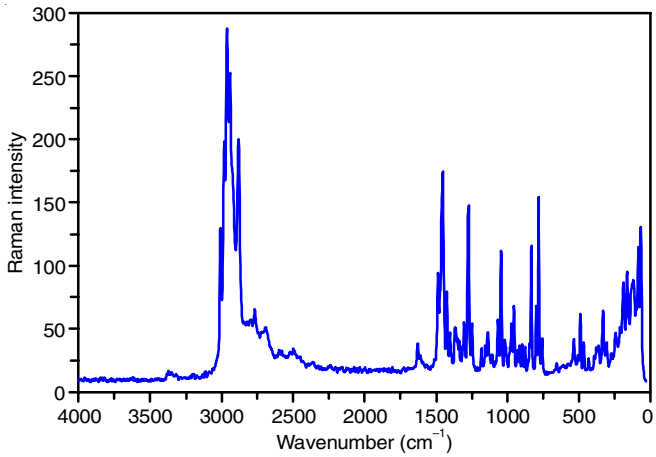

Fig. 3. Raman spectrum of **1**

Two IR peaks at 3538 and 3364 cm^{-1}, the Raman band at 3365 cm^{-1} and the near-IR peak at 1631 cm^{-1} were attributed to the ν(O–H) stretching and δ(H–O–H) bending modes of hydrated water molecules. The absorptions at 3220-3000 cm^{-1} and 3000-2685 cm^{-1} (IR and Raman, respectively) are assigned to the N–H and C–H stretching modes, respectively. The IR and Raman spectra of **1** show a series of absorption bands at 2600-2400 cm^{-1}, which are ascribed to the ν(NH_2^+) stretching vibrations as these bands were not observed in the IR spectra of free L. The absorption bands at ~2340 cm^{-1} in the IR spectrum of free L arise due to the asymmetric stretching mode of gaseous CO_2 and are related to background CO_2 in the IR spectrometer. The intense IR and Raman absorption bands at approximately 1600 cm^{-1} were assigned to the δ(NH_2^+) scissoring mode. For the $(CH_2)_n$ moieties in the compound, broad absorption bands were observed for the scissoring (1500-1400 cm^{-1}), wagging (1382-1170 cm^{-1}), twisting (1295-1063 cm^{-1}) and rocking (1174-724 cm^{-1}) motions [18-21].

Two very strong IR bands at 1490 and 1463 cm^{-1} and one Raman peak at 1467 cm^{-1} were ascribed to the δ(CH_2) bending mode. The ν(C–C) and ν(C–N) vibrational modes were observed in the region 1400-1000 cm^{-1}. The IR and Raman bands at 890-780 cm^{-1} were assigned to the rocking (ρ) motion of the NH_2 and CH_2 deformations. IR spectroscopy is useful in identifying geometric isomers of transition metal complexes with

TABLE-2
ASSIGNMENTS OF THE SELECTED BANDS OCCURRING IN THE IR and RAMAN SPECTRA OF **1**

IR bands (cm^{-1})	Raman bands (cm^{-1})	Assignments
3548 br, 3364 s	3365 w	ν(O–H)
3210 m	3190 w	ν_a(N–H)
3007 s	3104 w, 3051 w	ν_s(N–H)
2962 s,	2998 s, 2973 s, 2955 vs, 2933 s	ν_a(C–H)
2879 m, 2764 s, 2697 vs	2871 s, 2756 s, 2685 m	ν_s(C–H)
2597 s, 2527 m, 2496 s, 2450 m 2361 s, 2158 m	2595 w, 2509 w, 2484 w, 2436 w	
1631 sh		δ(H_2O)
1607 vs	1608 m	δ(NH_2^+) scissoring
1490 vs, 1463 vs	1467 s	δ(CH_2) scissoring
1424 m, 1413 s	1435 vs, 1405 s	
1396 s, 1380 s, 1362 s	1382 m	
1331 m, 1314 w	1328 w, 1317 w	ω(CH_2) wagging
1276 w, 1258 m	1280 m, 1252 vs	ω(CH_2) wagging
1238 m	1227 m	ν(C–N)
1180 s, 1162 w	1160 m	ν(C–C)
1136 w	1132 w	
1088 vs, 1136 w	1087 m, 1132 w	
1116 vs, 1101 s	1114 m	
1065 s, 1054 w	1083 w, 1042 m, 1020 s	τ(CH_2) twisting
999 vs, 980 m	994 m	ν_a(C–N)
954 m, 914 m	949 m, 932 m, 907 w	
878 m	892 m, 872 m	ν_s(C–N)
853 m, 846 m	853 m	ρ(NH_2^+) rocking
798 m, 782 w	809 s, 773 s	ρ(CH_2) rocking
760 m	756 vs, 731 m	
656 vs, 609 s	632 w	
568 vs, 535 vs	509 m	δ(CCN)
485 s	483 s	
445 s	439 m	
	403 w, 350 w, 213 m	
	181 w, 158 s, 132 s	

cyclam and cyclam derivatives. Due to its high symmetry, the IR absorption spectrum of the *trans*-isomer is simpler than that of the *cis*-isomer, resulting in two overlapping absorption bands near 890 cm^{-1} and a single peak near 800 cm^{-1}, arising from secondary amine and methylene vibrations, respectively. The *cis*-isomer exhibits at least three bands in the range 890-830 cm^{-1}, ascribed to the N–H wagging mode and the methylene vibration splits into two peaks in the range 830-790 cm^{-1} [22-27]. The strong IR absorptions at 1065, 1054 and 999 cm^{-1} and Raman bands at 1042, 1020 and 994 cm^{-1} appear in the CH_2 twisting region. The IR peak at 878 cm^{-1} and Raman band at 872 cm^{-1} are assigned to the NH_2^+ rocking vibration, while the two IR absorptions at 798 and 782 cm^{-1} and the Raman peak at 809 cm^{-1} are attributed to the CH_2 rocking vibration. The absorption positions of the bending (δ), wagging (ω), twisting (τ) and rocking (ρ) bands of the NH_2 and CH_2 deformations are not significantly affected by different counter anions [17-27]. However, the IR and Raman spectra did not provide any information on the exodentate conformations of the tetracationic macrocyclic rings in **1**. The UV-visible absorption spectrum

of **1** was acquired in MeOH; however, the tetra-protonated salt did not show any absorption band in the range 280-900 nm. Macrocyclic compound **1** was also EPR-silent.

X-ray structural characterization: Single-crystal X-ray diffraction analysis was performed to determine the exact conformation of the tetracationic compound **1** in the solid state. Compound **1** crystallized in the monoclinic space group $P2_1/n$ with two molecules of **1** in the unit cell [dimensions a = 7.5548(3) Å, b = 23.1838(8) Å, c = 8.3101(4) Å; β = 103.390(3)º]. The molecular structure of **1** along with the atom-numbering scheme is shown in Fig. 4.

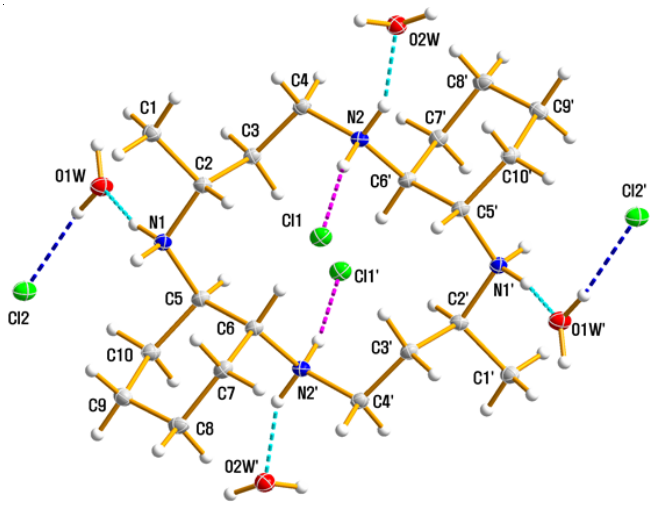

Fig. 4. Molecular structure of **1**, drawn with displacement ellipsoids at the 30% probability level. Dashed lines represent hydrogen bonding interactions and primed atoms are related by the symmetry code (-*x*+1, -*y*+1, -*z*+1)

The asymmetric unit consists of half a molecule of **1**, which lies across a crystallographic inversion center, along with two chloride counter ions and two lattice solvent water molecules. Selected bond lengths and bond angles and their standard deviations are listed in Table-3.

Within the centrosymmetric tetra-protonated amine unit, the C–C and N–C bond lengths range from 1.540(3) to 1.525(3) Å and 1.505(3) to 1.519(3) Å, respectively. The range of N–C–C and C–N–C angles are 106.82(19) to 114.52(19)º and 116.46(19) to 118.83(18)º, respectively. The bond lengths and angles within the tetracation $[C_{20}H_{44}N_4]^{4+}$ are comparable to those found in $[C_{20}H_{40}N_4]\cdot2(C_{10}H_7CH_2OH)$ [5], $[C_{20}H_{42}N_4](SO_4)\cdot2CH_3OH$ [6], $(C_{20}H_{42}N_4)\cdot2(NO_2OH)$ [7], $[C_{20}H_{42}N_4][Fe\{HB(pz)_3\}(CN)_3]_2\cdot2H_2O\cdot2CH_3OH$ [8], $[C_{20}H_{42}N_4]Br_2\cdot2H_2O$ [9] and $[C_{20}H_{44}N_4]Br_4\cdot4H_2O$ [9]. The four *N*-atoms are coplanar and the two methyl substituents are *anti* with respect to the macrocyclic plane as a result of the crystallographic inversion center. The six-membered cyclohexane ring is in a stable chair conformation. The organic $[C_{20}H_{44}N_4]^{4+}$ fragment adopts an exodentate [3,4,3,4]-*D* conformation. The exodentate rectangular conformation is quite different from the endodentate conformation of the free L or H_2L^{2+} exhibited in $(C_{20}H_{40}N_4)\cdot2(C_{10}H_7CH_2OH)$ [5], $(C_{20}H_{40}N_4)\cdot2(NO_2OH)$ [6], $[C_{20}H_{42}N_4](SO_4)\cdot2CH_3OH$ [7], $[C_{20}H_{42}N_4][Fe\{HB(pz)_3\}(CN)_3]_2\cdot2H_2O\cdot2CH_3OH$ [8] and $[C_{20}H_{42}N_4]Br_2\cdot2H_2O$ [9]. Two of the four nitrogen atoms, N1 and N1′ (symmetry generated) and two carbon atoms, C4 and C4′, establish the four corners of the macrocyclic square. The remaining two nitrogen atoms, N2 and N2′ and C atoms constitute the skeletal macrocyclic structure. The *exo* [3,4,3,4]-*D* conformation of **1** is also different from the *exo* [3,4,3,4]-*A* conformation of $(H_4cyclam)[HSO_4]_2$ [28] or $(H_4cyclam)[MnCl_4(H_2O)_2]Cl_2\cdot2H_2O$ [29], *exo* [3,4,3,4]-*B* conformation of $[H_4TMC](CrO_3Cl)_2Cl_2$ (TMC = 1,4,8,11-tetramethyl-1,4,8,11-tetraazacyclotetradecane) [30] and *exo* [3,4,3,4]-*C* conformations of $(H_4cyclam)[Cr_2O_7]_2\cdot H_2O$ [31] or $[H_4TMC](ClO_4)_2Cl_2$ [32].

Supramolecular features: Extensive O–H···Cl, N–H···Cl and N–H···O hydrogen-bonding interactions occur in the crystal structure as shown in Table-4. The chloride anions and the lattice water O atoms serve as hydrogen-bond acceptors, while the macrocycle N–H groups and the water molecule O–H groups act as donors. The organic $[C_{20}H_{44}N_4]^{4+}$ cation participates in hydrogen bonding with water molecules and chloride ions through N–H···O and N–H···Cl interactions. The chloride ions extend the hydrogen bonding network *via* water O–H···Cl interactions. The hydrogen atoms on N1 and N2 both forms bifurcated hydrogen bonds with the O and Cl atoms. An extensive array of these contacts generates a 3D network of hydrogen-bonded molecules, which help to stabilize the crystal structure. A detailed understanding and insight into the crystal packing and conformation may be helpful in the development of new anti-HIV drugs.

TABLE-3
SELECTED BOND DISTANCES (Å) AND ANGLES (°) FOR **1**

N1–C2	1.519 (3)	C5–C6	1.540 (3)
N1–C5	1.509 (3)	C5–C10	1.536 (3)
N2–C4	1.505 (3)	C6–C7	1.525 (3)
N2–C6^{i}	1.510 (3)	C7–C8	1.532 (4)
C1–C2	1.525 (3)	C8–C9	1.525 (4)
C2–C3	1.533 (3)	C9–C10	1.537 (4)
C3–C4	1.525 (3)		
C5–N1–C2	118.83 (18)	C10–C5–C6	112.61 (19)
C4–N2–C6^{i}	116.46 (19)	N2^{i}–C6–C5	106.82 (19)
N1–C2–C1	107.06 (19)	N2^{i}–C6–C7	111.96 (19)
N1–C2–C3	110.43 (19)	C7–C6–C5	111.9 (2)
C1–C2–C3	112.12 (19)	C6–C7–C8	111.7 (2)
C4–C3–C2	113.50 (2)	C9–C8–C7	111.0 (2)
N2–C4–C3	114.52 (19)	C8–C9–C10	111.9 (2)
N1–C5–C6	110.95 (19)	C5–C10–C9	114.0 (2)
N1–C5–C10	109.48 (19)		

Symmetry code: (i) –*x*+1, -*y*+1, -*z*+1

TABLE-4
HYDROGEN BOND PARAMETERS (Å,°) FOR **1**

D–H···A	D–H	H···A	D···A	D–H···A
O1*W*–H1*WA*···Cl2	0.87	2.27	3.130 (2)	172
O1*W*–H1*WB*···Cl2^{ii}	0.87	2.32	3.1897 (19)	174
O2*W*–H2*WA*···Cl2^{iii}	0.87	2.29	3.1508 (19)	173
O2*W*–H2*WB*···Cl1^{iv}	0.87	2.24	3.0923 (19)	167
N1–H1*A*···Cl2^{v}	0.91	2.41	3.291 (2)	164
N1–H1*B*···O1*W*	0.91	1.84	2.720 (3)	163
N2–H2*A*···Cl1	0.91	2.21	3.107 (2)	170
N2–H2*B*···O2*W*	0.91	1.88	2.739 (3)	156

Symmetry code: (ii) *x*-1/2, -*y*+3/2, *z*-1/2; (iii) -*x*+1/2, *y*-1/2, -*z*+1/2; (iv) –*x*+1, -*y*+1, -*z*; (v) *x*+1/2, -*y*+3/2, *z*-1/2.

Hirshfeld surface analysis: Hirshfeld surfaces [33] and their relative 2D fingerprint plots [34] were drawn using CrystalExplorer [34]. The three-dimensional d_{norm} surface shows negative values for short intermolecular contacts and positive values for contacts that are longer than the sum of the van der Waals (vdW) radii [33,34]. The Hirshfeld surfaces of **1** are depicted in Fig. 5, wherein the surfaces mapped around the molecule by the d_{norm} surface, shape index and curvedness are presented.

The d_{norm} surface identifies the close intermolecular interactions. In contrast, the shape index is most sensitive to subtle changes in the surface shape. Curvedness provides the shape of the molecules. The flat areas of the surface indicate low curvedness values, whereas sharp areas indicate high curvedness. The d_{norm} values were mapped onto the Hirshfeld surface, with the red regions representing close contacts and negative d_{norm}, white regions showing contacts close to the vdW separation and blue regions depicting long contacts (> vdW radii) and positive d_{norm}. The surface is usually divided into patches to indicate interactions between neighboring molecules. The d_{norm} surface shows red, white and blue spots for contacts resulting from H···H, H···Cl and H···O interactions, respectively. The 2-D fingerprint plots provide information regarding the overall contribution of intermolecular contacts and their percentage distributions on the Hirshfeld surface [34]. The Hirshfeld surface contours and 2-D fingerprint plots of various interactions are shown in Figs. 6-9, with d_i defined as the closest internal distance from a given point on the Hirshfeld surface and d_e the closest external contact [35-40]. The most significant contribution comes from H···H (60.6%) contacts, followed by H···Cl interactions (34.7%), which are responsible for the appearance of red spots and correlate with the O–H···Cl hydrogen bonds. The contribution of H···O (4.7%) interactions is also observed, while that of other contact types is negligible. The high percentages of H···H, H···Cl and H···O contacts suggest that vdW and hydrogen bonding interactions play a major role in the molecular packing, which is consistent with the crystal packing topology.

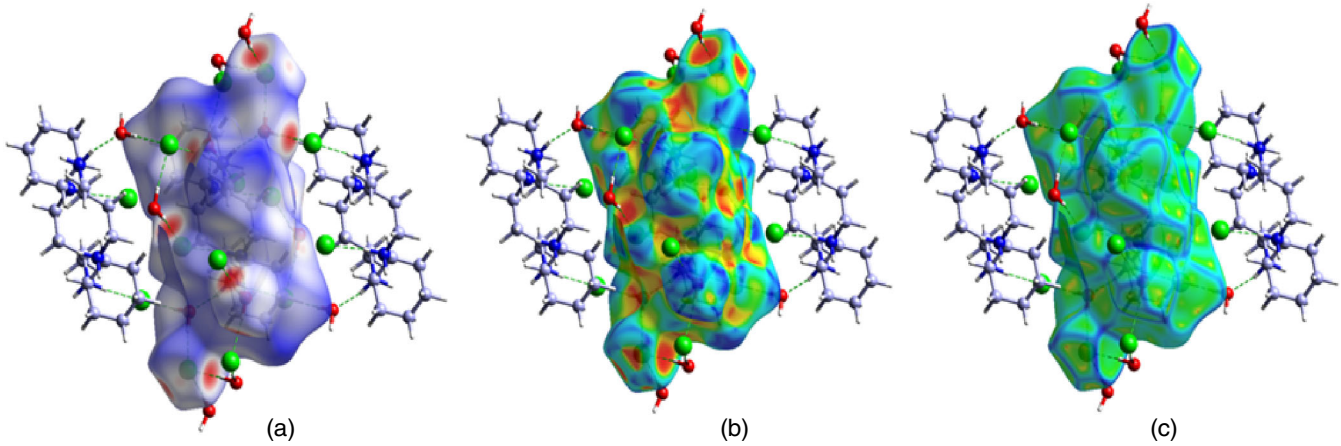

Fig. 5. Hirshfeld surfaces mapped with (a) d_{norm}, (b) shape index and (c) curvedness

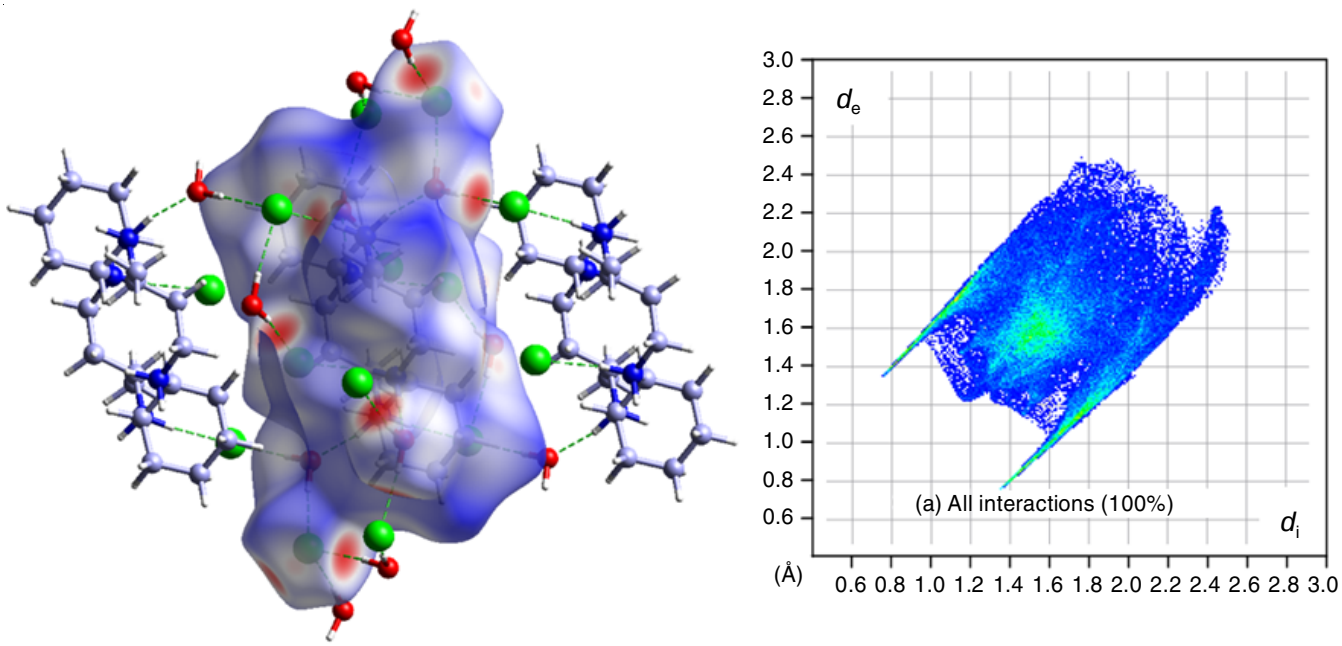

Fig. 6. Hirshfeld surface mapped with (left) d_{norm} and 2D fingerprint map (right) for (a) all interactions

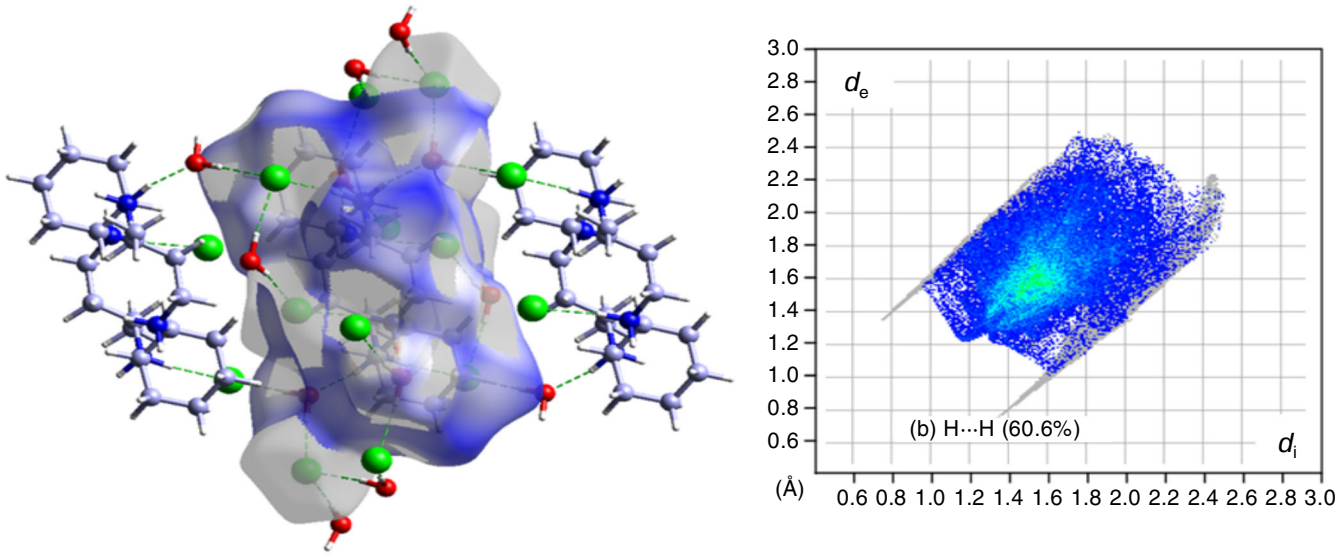

Fig. 7. Hirshfeld surface mapped with (left) d_{norm} and 2D fingerprint plot (right) for (b) H···H interaction

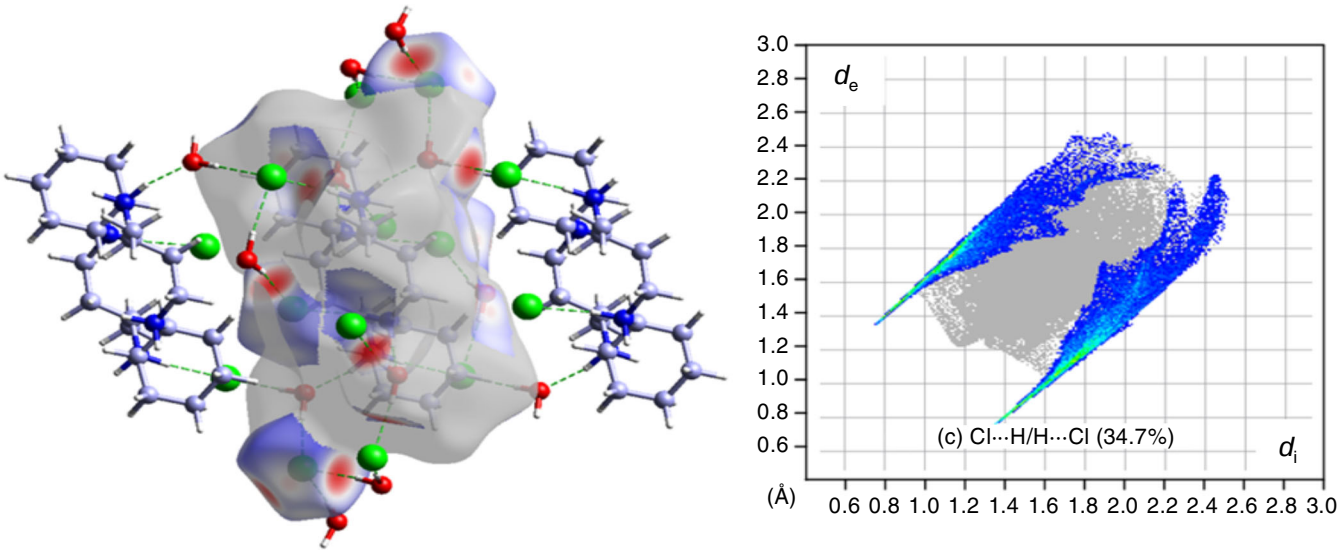

Fig. 8. Hirshfeld surface mapped with (left) d_{norm} and 2D fingerprint plot (right) for (c) Cl···H/H···Cl interactions

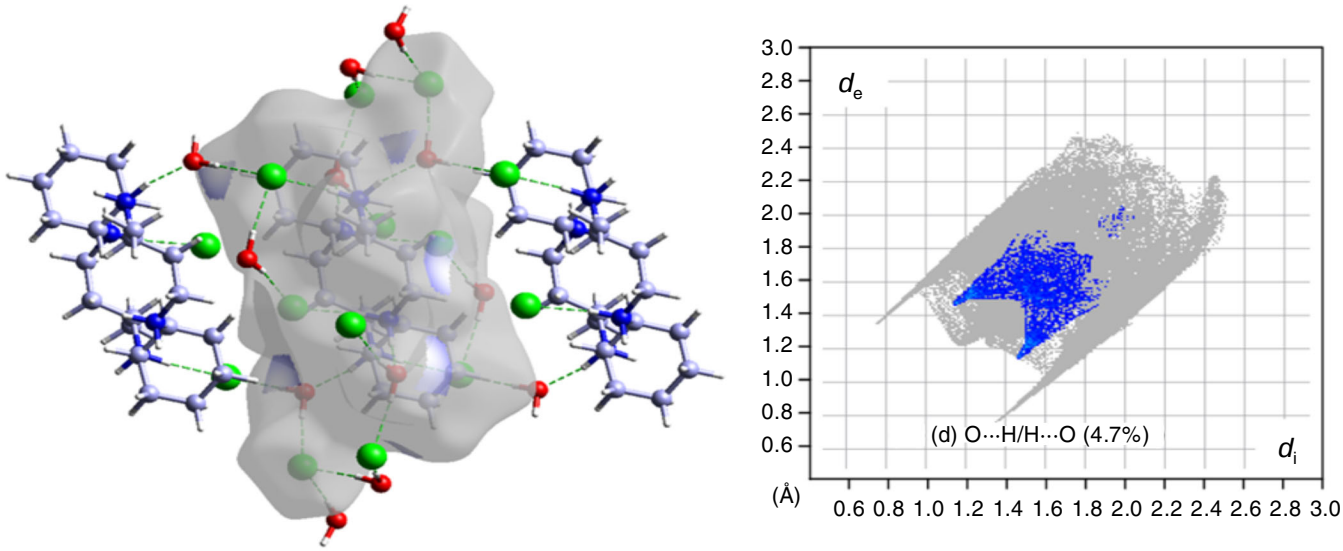

Fig. 9. Hirshfeld surface mapped with (left) d_{norm} and 2D fingerprint plot (right) for (d) O···H/H···O interactions

Conclusion

Suitable single crystals of compound **1** for structural analysis using a conventional X-ray diffractometer were obtained by a new synthetic method. Compound **1** was characterized by elemental analysis, spectroscopic methods and single-crystal X-ray diffraction analysis. The asymmetric unit of **1** contains one half of the centrosymmetric $[C_{20}H_{44}N_4]^{4+}$ cation, two chloride anions and two water molecules. The tetra-protonated organic cation adopts the [3,4,3,4]-*D* exodentate conformation as a consequence of intermolecular hydrogen bonds between chloride anions and hydrated water molecules. The N–H···Cl and N–H···O hydrogen bonds interconnect macrocyclic tetracations with water molecules and chloride anions, giving rise to a three-dimensional network of molecules. These hydrogen-bonding interactions help to stabilize the crystal structure. Investigation of intermolecular interactions and crystal packing *via* Hirshfeld surface analysis indicate that H···H, Cl···H/H···Cl and O···H/H···O contacts are the most abundant in the solid-state structure.

Supplementary material

Crystallographic data for the structures reported here have been deposited with CCDC Deposition No 2036961. These data can be obtained free of charge from the Cambridge Crystallographic Data Centre, 12 Union Road, Cambridge CB2 1EZ, UK, Fax: +441223336033; E-mail: deposit@ccdc.cam.ac.uk.

ACKNOWLEDGEMENTS

This work was supported by a Research Grant of Andong National University.

CONFLICT OF INTEREST

The authors declare that there is no conflict of interests regarding the publication of this article.

REFERENCES

1. G.C. Valks, G. McRobbie, E.A. Lewis, T.J. Hubin, T.M. Hunter, P.J. Sadler, C. Pannecouque, E. De Clercq and S.J. Archibald, *J. Med. Chem.*, **49**, 6162 (2006); https://doi.org/10.1021/jm0607810
2. L. Ronconi and P.J. Sadler, *Coord. Chem. Rev.*, **251**, 1633 (2007); https://doi.org/10.1016/j.ccr.2006.11.017
3. A. Ross, J.-H. Choi, T.M. Hunter, C. Pannecouque, S.A. Moggach, S. Parsons, E. De Clercq and P.J. Sadler, *Dalton Trans.*, **41**, 6408 (2012); https://doi.org/10.1039/c2dt30140g
4. E. De Clercq, *J. Med. Chem.*, **53**, 1438 (2010); https://doi.org/10.1021/jm900932g
5. J.-H. Choi, M.A. Subhan, K.S. Ryoo and S.W. Ng, *Acta Crystallogr. Sect. E*, **68**, o102 (2012); https://doi.org/10.1107/S160053681105272X
6. D. Moon, S. Jeon, K.S. Ryoo and J.-H. Choi, *Asian J. Chem.*, **32**, 697 (2020); https://doi.org/10.14233/ajchem.2020.22506
7. F. White, P.J. Sadler and M. Melchart, *CSD Communication* CCDC 1408165 (2015).
8. J. Kim, S. Han, I.-K. Cho, K.Y. Choi, M. Heu, S. Yoon and B.J. Suh, *Polyhedron*, **23**, 1333 (2004); https://doi.org/10.1016/j.poly.2004.02.026
9. D. Moon, S. Jeon and J.-H. Choi, *J. Mol. Struct.*, **1232**, 130011 (2021); https://doi.org/10.1016/j.molstruc.2021.130011
10. D. Moon and J.-H. Choi, *Acta Crystallogr. Sect E*, **74**, 1039 (2018); https://doi.org/10.1107/S2056989018009337
11. S.G. Kang, J.K. Kweon and S.K. Jung, *Bull. Korean Chem. Soc.*, **12**, 483 (1991).
12. S. Jeon, J. Moncol, M. Mazúr, M. Valko and J.-H. Choi, *Crystals*, **9**, 336 (2019); https://doi.org/10.3390/cryst9070336
13. G.M. Sheldrick, *Acta Crystallogr. Sect. A*, **71**, 3 (2015); https://doi.org/10.1107/S2053273314026370
14. G.M. Sheldrick, *Acta Crystallogr. Sect. C*, **71**, 3 (2015); https://doi.org/10.1107/S2053229614024218
15. J. Koziskova, F. Hahn, J. Richter and J. Kozisek, *Acta Chim. Slov.*, **9**, 136 (2016); https://doi.org/10.1515/acs-2016-0023
16. K. Brandenburg and H. Putz, DIAMOND-3, University of Bonn, Bonn, Germany (2014).
17. J.-H. Choi, W. Clegg, G.S. Nichol, S.H. Lee, Y.C. Park and M.H. Habibi, *Spectrochim. Acta A Mol. Biomol. Spectrosc.*, **68**, 796 (2007); https://doi.org/10.1016/j.saa.2007.01.002
18. J.-H. Choi and S.H. Lee, *J. Mol. Struct.*, **932**, 84 (2009); https://doi.org/10.1016/j.molstruc.2009.05.048
19. D. Moon and J.-H. Choi, *Spectrochim. Acta A Mol. Biomol. Spectrosc.*, **138**, 774 (2015); https://doi.org/10.1016/j.saa.2014.11.099
20. T. Aree, Y.P. Hong and J.-H. Choi, *J. Mol. Struct.*, **1163**, 86 (2018); https://doi.org/10.1016/j.molstruc.2018.02.102
21. D. Moon and J.-H. Choi, *Inorg. Chim. Acta*, **519**, 120259 (2021); https://doi.org/10.1016/j.ica.2021.120259
22. J.-H. Choi, *Chem. Phys.*, **256**, 29 (2000); https://doi.org/10.1016/S0301-0104(00)00097-5
23. J.-H. Choi, *Spectrochim. Acta A Mol. Biomol. Spectrosc.*, **56**, 1653 (2000); https://doi.org/10.1016/S1386-1425(00)00221-3
24. J.-H. Choi, I.G. Oh, T. Suzuki and S. Kaizaki, *J. Mol. Struct.*, **694**, 39 (2004); https://doi.org/10.1016/j.molstruc.2004.01.034
25. J.-H. Choi, *Inorg. Chim. Acta*, **362**, 4231 (2009); https://doi.org/10.1016/j.ica.2009.05.024
26. D. Moon, M. Mazúr, M. Valko and J.-H. Choi, *J. Mol. Struct.*, **1221**, 128711 (2020); https://doi.org/10.1016/j.molstruc.2020.128711
27. D. Moon and J.-H. Choi, *J. Coord. Chem.*, **74**, 969 (2021); https://doi.org/10.1080/00958972.2020.1863381
28. S. Said, N. Mhadhbi, F. Hajlaoui, T. Bataille and H. Naïli, *Acta Crystallogr. Sect. E*, **69**, o1278 (2013); https://doi.org/10.1107/S1600536813018953
29. M. Pojarová, K. Fejfarová and B. El Bali, *Acta Crystallogr. Sect. E*, **66**, m1103 (2013); https://doi.org/10.1107/S1600536810031958
30. D. Moon and J.-H. Choi, *Acta Crystallogr. Sect. E*, **76**, 523 (2020); https://doi.org/10.1107/S2056989020003059
31. D. Moon and J.-H. Choi, *Acta Crystallogr. Sect. E*, **73**, 755 (2017); https://doi.org/10.1107/S2056989017005771
32. D. Moon and J.-H. Choi, *Acta Crystallogr. Sect. E*, **76**, 324 (2020); https://doi.org/10.1107/S2056989020001322
33. J.J. McKinnon, D. Jayatilaka and M.A. Spackman, *Chem. Commun.*, 3814 (2007); https://doi.org/10.1039/b704980c
34. M.A. Spackman and J.J. McKinnon, *CrystEngComm*, **4**, 378 (2002); https://doi.org/10.1039/B203191B
35. M.J. Turner, J.J. McKinnon, S.K. Wolff, D.J. Grimwood, P.R. Spackman, D. Jayatilaka and M.A. Spackman, CrystalExplorer17, University of Western Australia (2017).
36. M.A. Spackman and D. Jayatilaka, *CrystEngComm*, **11**, 19 (2009); https://doi.org/10.1039/B818330A
37. D. Moon, S. Tanaka, T. Akitsu and J.-H. Choi, *J. Mol. Struct.*, **1154**, 338 (2018); https://doi.org/10.1016/j.molstruc.2017.10.066
38. J. Moncol, M. Mazúr, M. Valko and J.-H. Choi, *Acta Crystallogr. Sect. C*, **75**, 616 (2019); https://doi.org/10.1107/S2053229619005588
39. D. Moon, J. Jeon and J.-H. Choi, *J. Coord. Chem.*, **73**, 2029 (2020); https://doi.org/10.1080/00958972.2020.1799199
40. D. Moon, S. Jeon, M. Mazúr, M. Valko and J.-H. Choi, *J. Mol. Struct.*, **1231**, 129897 (2021); https://doi.org/10.1016/j.molstruc.2021.129897